Eur. Phys. J. C 18, 447–460 (2001)
Digital Object Identifier (DOI) 10.1007/s100520100580

THE EUROPEAN PHYSICAL JOURNAL C

Production rates of $b\bar{b}$ quark pairs from gluons and $b\bar{b}b\bar{b}$ events in hadronic Z^0 decays

The OPAL Collaboration

G. Abbiendi[2], K. Ackerstaff[8], C. Ainsley[5], P.F. Akesson[3], G. Alexander[22], J. Allison[16], K.J. Anderson[9], S. Arcelli[17], S. Asai[23], S.F. Ashby[1], D. Axen[27], G. Azuelos[18,a], I. Bailey[26], A.H. Ball[8], E. Barberio[8], R.J. Barlow[16], S. Baumann[3], T. Behnke[25], K.W. Bell[20], G. Bella[22], A. Bellerive[9], S. Bentvelsen[8], S. Bethke[14,i], O. Biebel[14,i], I.J. Bloodworth[1], P. Bock[11], J. Böhme[14,h], O. Boeriu[10], D. Bonacorsi[2], M. Boutemeur[31], S. Braibant[8], P. Bright-Thomas[1], L. Brigliadori[2], R.M. Brown[20], H.J. Burckhart[8], J. Cammin[3], P. Capiluppi[2], R.K. Carnegie[6], A.A. Carter[13], J.R. Carter[5], C.Y. Chang[17], D.G. Charlton[1,b], C. Ciocca[2], P.E.L. Clarke[15], E. Clay[15], I. Cohen[22], O.C. Cooke[8], J. Couchman[15], C. Couyoumtzelis[13], R.L. Coxe[9], M. Cuffiani[2], S. Dado[21], G.M. Dallavalle[2], S. Dallison[16], A. de Roeck[8], P. Dervan[15], K. Desch[25], B. Dienes[30,h], M.S. Dixit[7], M. Donkers[6], J. Dubbert[31], E. Duchovni[24], G. Duckeck[31], I.P. Duerdoth[16], P.G. Estabrooks[6], E. Etzion[22], F. Fabbri[2], M. Fanti[2], L. Feld[10], P. Ferrari[12], F. Fiedler[8], I. Fleck[10], M. Ford[5], A. Frey[8], A. Fürtjes[8], D.I. Futyan[16], P. Gagnon[12], J.W. Gary[4], G. Gaycken[25], C. Geich-Gimbel[3], G. Giacomelli[2], P. Giacomelli[8], D. Glenzinski[9], J. Goldberg[21], C. Grandi[2], K. Graham[26], E. Gross[24], J. Grunhaus[22], M. Gruwé[25], P.O. Günther[3], C. Hajdu[29], G.G. Hanson[12], M. Hansroul[8], M. Hapke[13], K. Harder[25], A. Harel[21], C.K. Hargrove[7], M. Harin-Dirac[4], A. Hauke[3], M. Hauschild[8], C.M. Hawkes[1], R. Hawkings[25], R.J. Hemingway[6], C. Hensel[25], G. Herten[10], R.D. Heuer[25], M.D. Hildreth[8], J.C. Hill[5], A. Hocker[9], K. Hoffman[8], R.J. Homer[1], A.K. Honma[8], D. Horváth[29,c], K.R. Hossain[28], R. Howard[27], P. Hüntemeyer[25], P. Igo-Kemenes[11], K. Ishii[23], F.R. Jacob[20], A. Jawahery[17], H. Jeremie[18], C.R. Jones[5], P. Jovanovic[1], T.R. Junk[6], N. Kanaya[23], J. Kanzaki[23], G. Karapetian[18], D. Karlen[6], V. Kartvelishvili[16], K. Kawagoe[23], T. Kawamoto[23], R.K. Keeler[26], R.G. Kellogg[17], B.W. Kennedy[20], D.H. Kim[19], K. Klein[11], A. Klier[24], T. Kobayashi[23], M. Kobel[3], T.P. Kokott[3], S. Komamiya[23], R.V. Kowalewski[26], T. Kress[4], P. Krieger[6], J. von Krogh[11], T. Kuhl[3], M. Kupper[24], P. Kyberd[13], G.D. Lafferty[16], H. Landsman[21], D. Lanske[14], I. Lawson[26], J.G. Layter[4], A. Leins[31], D. Lellouch[24], J. Letts[12], L. Levinson[24], R. Liebisch[11], J. Lillich[10], B. List[8], C. Littlewood[5], A.W. Lloyd[1], S.L. Lloyd[13], F.K. Loebinger[16], G.D. Long[26], M.J. Losty[7], J. Lu[27], J. Ludwig[10], A. Macchiolo[18], A. Macpherson[28], W. Mader[3], M. Mannelli[8], S. Marcellini[2], T.E. Marchant[16], A.J. Martin[13], J.P. Martin[18], G. Martinez[17], T. Mashimo[23], P. Mättig[24], W.J. McDonald[28], J. McKenna[27], T.J. McMahon[1], R.A. McPherson[26], F. Meijers[8], P. Mendez-Lorenzo[31], F.S. Merritt[9], H. Mes[7], A. Michelini[2], S. Mihara[23], G. Mikenberg[24], D.J. Miller[15], W. Mohr[10], A. Montanari[2], T. Mori[23], K. Nagai[8], I. Nakamura[23], H.A. Neal[12,f], R. Nisius[8], S.W. O'Neale[1], F.G. Oakham[7], F. Odorici[2], H.O. Ogren[12], A. Oh[8], A. Okpara[11], M.J. Oreglia[9], S. Orito[23], G. Pásztor[8,j], J.R. Pater[16], G.N. Patrick[20], J. Patt[10], P. Pfeifenschneider[14], J.E. Pilcher[9], J. Pinfold[28], D.E. Plane[8], B. Poli[2], J. Polok[8], O. Pooth[8], M. Przybycień[8,d], A. Quadt[8], C. Rembser[8], H. Rick[4], S.A. Robins[21], N. Rodning[28], J.M. Roney[26], S. Rosati[3], K. Roscoe[16], A.M. Rossi[2], Y. Rozen[21], K. Runge[10], O. Runolfsson[8], D.R. Rust[12], K. Sachs[6], T. Saeki[23], O. Sahr[31], E.K.G. Sarkisyan[22], C. Sbarra[26], A.D. Schaile[31], O. Schaile[31], P. Scharff-Hansen[8], S. Schmitt[11], M. Schröder[8], M. Schumacher[25], C. Schwick[8], W.G. Scott[20], R. Seuster[14,h], T.G. Shears[8], B.C. Shen[4], C.H. Shepherd-Themistocleous[5], P. Sherwood[15], G.P. Siroli[2], A. Skuja[17], A.M. Smith[8], G.A. Snow[17], R. Sobie[26], S. Söldner-Rembold[10,e], S. Spagnolo[20], M. Sproston[20], A. Stahl[3], K. Stephens[16], K. Stoll[10], D. Strom[19], R. Ströhmer[31], B. Surrow[8], S.D. Talbot[1], S. Tarem[21], R.J. Taylor[15], R. Teuscher[9], M. Thiergen[10], J. Thomas[15], M.A. Thomson[8], E. Torrence[9], S. Towers[6], T. Trefzger[31], I. Trigger[8], Z. Trócsányi[30,g], E. Tsur[22], M.F. Turner-Watson[1], I. Ueda[23], P. Vannerem[10], M. Verzocchi[8], H. Voss[8], J. Vossebeld[8], D. Waller[6], C.P. Ward[5], D.R. Ward[5], P.M. Watkins[1], A.T. Watson[1], N.K. Watson[1], P.S. Wells[8], T. Wengler[8], N. Wermes[3], D. Wetterling[11] J.S. White[6], G.W. Wilson[16], J.A. Wilson[1], T.R. Wyatt[16], S. Yamashita[23], V. Zacek[18], D. Zer-Zion[8]

[1] School of Physics and Astronomy, University of Birmingham, Birmingham B15 2TT, UK
[2] Dipartimento di Fisica dell' Università di Bologna and INFN, 40126 Bologna, Italy
[3] Physikalisches Institut, Universität Bonn, 53115 Bonn, Germany
[4] Department of Physics, University of California, Riverside CA 92521, USA
[5] Cavendish Laboratory, Cambridge CB3 0HE, UK
[6] Ottawa-Carleton Institute for Physics, Department of Physics, Carleton University, Ottawa, Ontario K1S 5B6, Canada
[7] Centre for Research in Particle Physics, Carleton University, Ottawa, Ontario K1S 5B6, Canada
[8] CERN, European Organisation for Nuclear Research, 1211 Geneva 23, Switzerland
[9] Enrico Fermi Institute and Department of Physics, University of Chicago, Chicago IL 60637, USA

[10] Fakultät für Physik, Albert Ludwigs Universität, 79104 Freiburg, Germany
[11] Physikalisches Institut, Universität Heidelberg, 69120 Heidelberg, Germany
[12] Indiana University, Department of Physics, Swain Hall West 117, Bloomington IN 47405, USA
[13] Queen Mary and Westfield College, University of London, London E1 4NS, UK
[14] Technische Hochschule Aachen, III Physikalisches Institut, Sommerfeldstrasse 26-28, 52056 Aachen, Germany
[15] University College London, London WC1E 6BT, UK
[16] Department of Physics, Schuster Laboratory, The University, Manchester M13 9PL, UK
[17] Department of Physics, University of Maryland, College Park, MD 20742, USA
[18] Laboratoire de Physique Nucléaire, Université de Montréal, Montréal, Quebec H3C 3J7, Canada
[19] University of Oregon, Department of Physics, Eugene OR 97403, USA
[20] CLRC Rutherford Appleton Laboratory, Chilton, Didcot, Oxfordshire OX11 0QX, UK
[21] Department of Physics, Technion-Israel Institute of Technology, Haifa 32000, Israel
[22] Department of Physics and Astronomy, Tel Aviv University, Tel Aviv 69978, Israel
[23] International Centre for Elementary Particle Physics and Department of Physics, University of Tokyo, Tokyo 113-0033, and Kobe University, Kobe 657-8501, Japan
[24] Particle Physics Department, Weizmann Institute of Science, Rehovot 76100, Israel
[25] Universität Hamburg/DESY, II Institut für Experimental Physik, Notkestrasse 85, 22607 Hamburg, Germany
[26] University of Victoria, Department of Physics, P O Box 3055, Victoria BC V8W 3P6, Canada
[27] University of British Columbia, Department of Physics, Vancouver BC V6T 1Z1, Canada
[28] University of Alberta, Department of Physics, Edmonton AB T6G 2J1, Canada
[29] Research Institute for Particle and Nuclear Physics, 1525 Budapest, P O Box 49, Hungary
[30] Institute of Nuclear Research, 4001 Debrecen, P O Box 51, Hungary
[31] Ludwigs-Maximilians-Universität München, Sektion Physik, Am Coulombwall 1, 85748 Garching, Germany

Received: 9 June 2000 / Published online: 23 January 2001 –

Abstract. The rates are measured per hadronic Z^0 decay for gluon splitting to $b\bar{b}$ quark pairs, $g_{b\bar{b}}$, and of events containing two $b\bar{b}$ quark pairs, g_{4b}, using a sample of four-jet events selected from data collected with the OPAL detector. Events with an enhanced signal of gluon splitting to $b\bar{b}$ quarks are selected if two of the jets are close in phase-space and contain detached secondary vertices. For the event sample containing two $b\bar{b}$ quark pairs, three of the four jets are required to have a significantly detached secondary vertex. Information from the event topology is combined in a likelihood fit to extract the values of $g_{b\bar{b}}$ and g_{4b}, namely

$$g_{b\bar{b}} = (3.07 \pm 0.53(\text{stat}) \pm 0.97(\text{syst})) \times 10^{-3},$$
$$g_{4b} = (0.36 \pm 0.17(\text{stat}) \pm 0.27(\text{syst})) \times 10^{-3}.$$

1 Introduction

Bottom quark pairs in Z^0 decays can be produced either directly via $Z^0 \to b\bar{b}$ or indirectly, when a gluon is radiated from a quark and then splits into a $b\bar{b}$ quark pair. A special case consists of events with both direct and indirect b quark production, $Z^0 \to b\bar{b}g \to b\bar{b}b\bar{b}$. The rates $g_{b\bar{b}}$ and g_{4b} per hadronic Z^0 decay, for the reactions $Z^0 \to q\bar{q}g$ with $g \to b\bar{b}$ and $Z^0 \to b\bar{b}b\bar{b}$ are sensitive to both the b quark mass and the strong coupling constant α_s. Hence measurements of these rates are tests of the theory of Quantum Chromodynamics (QCD). Events with gluon splitting into $b\bar{b}$ quark pairs are an important background for the measurement of R_b, the fraction of hadronic Z^0 decays into $b\bar{b}$ quark pairs. Therefore, a more precise determination of $g_{b\bar{b}}$ might lead to a reduction of the systematic uncertainty in R_b.

The rate $g_{b\bar{b}}$ has been calculated in [1,2], including the re-summation of leading logarithmic terms. Those authors point out that the parton-shower approach as implemented e.g. in JETSET 7.4 [3] is a good approximation. Numerical calculations of $g_{b\bar{b}}$ are given in [1,2,4], predicting a rate in the range $g_{b\bar{b}}^{\text{theor}} = (1.8 - 2.9) \times 10^{-3}$, depending on the b quark mass and the strong coupling constant.

An estimate of g_{4b} can be obtained from the rate for direct $b\bar{b}$ production, R_b, multiplied by the rate of indirect $b\bar{b}$ production, $g_{b\bar{b}}$. This simple picture is modified because the phase-space for two $b\bar{b}$ quark pairs is smaller than that for two light and two b quarks. The interference between secondary $b\bar{b}$ production and primary $b\bar{b}$ production cancels to zero at leading order in α_s, except for

[a] and at TRIUMF, Vancouver, Canada V6T 2A3
[b] and Royal Society University Research Fellow
[c] and Institute of Nuclear Research, Debrecen, Hungary
[d] and University of Mining and Metallurgy, Cracow
[e] and Heisenberg Fellow
[f] now at Yale University, Dept of Physics, New Haven, USA
[g] and Department of Experimental Physics, Lajos Kossuth University, Debrecen, Hungary
[h] and MPI München
[i] now at MPI für Physik, 80805 München
[j] and Research Institute for Particle and Nuclear Physics, Budapest, Hungary

the $b\bar{b}b\bar{b}$ final state [1,5]. In [1], the contribution of this interference term is shown to be less than 0.2% of $g_{b\bar{b}}$.

Measurements of $g_{b\bar{b}}$ using four-jet final states have been reported by the DELPHI and ALEPH collaborations, with the results $g_{b\bar{b}} = (2.1 \pm 1.1(\text{stat}) \pm 0.9(\text{syst})) \times 10^{-3}$ [6] and $g_{b\bar{b}} = (2.77 \pm 0.42(\text{stat}) \pm 0.57(\text{syst})) \times 10^{-3}$ [7], respectively, in agreement with theoretical predictions. A measurement of the $b\bar{b}b\bar{b}$ final state in a three jet topology has recently been presented by DELPHI [8], with the result $g_{4b} = (0.60 \pm 0.19(\text{stat}) \pm 0.14(\text{syst})) \times 10^{-3}$. This result is translated into a gluon splitting rate $g_{b\bar{b}} = (3.3 \pm 1.0(\text{stat}) \pm 0.8(\text{syst})) \times 10^{-3}$, using a tree-level QCD calculation for the ratio $g_{b\bar{b}}/g_{4b}$. The calculation was carried out by DELPHI [8], using the WPHACT 1.3 Monte Carlo generator [9].

In this analysis, decays of the Z^0 into four-jet final states are investigated. Jets from b or $\bar{b}$ quarks are identified by reconstructing secondary decay vertices. The invariant mass of $b\bar{b}$ quark pairs originating from gluons tends to peak just above threshold. This leads to a small relative momentum of the two b hadrons produced in the fragmentation process. By contrast, directly produced $b\bar{b}$ quark pairs have high invariant masses, since they carry a large part of the Z^0 energy. This and other characteristics are used to select event samples enriched in the process $g \to b\bar{b}$. An angular correlation defined similarly to the Bengtsson-Zerwas angle [10] is used to further differentiate between $q\bar{q}q\bar{q}$ and $q\bar{q}gg$ final states. In addition, events with three reconstructed secondary vertices are selected. They are used to measure the g_{4b} rate.

2 Event selection and reconstruction

2.1 The OPAL detector

The OPAL detector is described in detail elsewhere [11]. Only a brief description of the detector elements relevant to this analysis is given here. Charged tracks are reconstructed in the central tracking system. It consists of a silicon microvertex detector, a vertex drift chamber equipped with axial and stereo wires, a large jet chamber and z chambers[1]. A solenoid providing a uniform magnetic field of 0.435 T parallel to the z-axis surrounds the central tracking system. The silicon microvertex detector [12] has two layers which measure tracks in (r, ϕ). This detector was upgraded in 1993 to provide a precise measurement of the z coordinate [13]. Before this detector was upgraded again in 1995 for the high energy operation in the LEP 2 programme [14] the inner layer covered the range $|\cos(\theta)| < 0.83$ and the outer layer the range $|\cos(\theta)| < 0.77$. The vertex chamber extends over the range $|\cos\theta| < 0.95$. The coil is surrounded by scintillators for time-of-flight measurements and a barrel lead-glass electromagnetic calorimeter. Including the endcap electromagnetic calorimeter, the lead-glass blocks cover the range $|\cos\theta| < 0.98$. The magnetic return yoke is instrumented with streamer tubes and serves as a hadron calorimeter. The return yoke in turn is surrounded by muon chambers.

[1] The OPAL coordinate system is defined with positive z-axis along the electron beam direction, the x axis pointing to the center of the LEP accelerator ring and the y-axis normal to the x–z plane. The polar and azimuthal angles are denoted by θ and ϕ, respectively

2.2 Event selection and reconstruction

The analysis uses data taken with the OPAL detector in the years 1992–1995 on or near the Z^0 resonance. Hadronic Z^0 decays are selected with an efficiency of 98.4%, as described in [15]. Only events with the tracking system and the electromagnetic calorimeter fully operational are used in this analysis. A total number of 3.35 million hadronic events are selected. In these events well-measured charged tracks are used with a momentum $p_t > 0.15\,\text{GeV}/c$ in the (x, y) plane, and clusters in the electromagnetic calorimeter with energies above 0.1 GeV (0.25 GeV) in the barrel (end-cap) region. The energies of clusters pointed to by charged tracks are corrected for double counting by subtracting the energy deposition expected from the track momentum [16].

2.3 Simulated events

A total number of 150 000 events generated with PYTHIA 6.130 [17] and 14 million events generated with JETSET 7.4 [3] are used to evaluate the efficiencies for signal and background, respectively. Within the JETSET 7.4 sample, 4.3 million (1.9 million) events were generated in special runs with a primary $b\bar{b}$ ($c\bar{c}$) quark pair to increase the statistical significance of the description of background processes with secondary decay vertices. To study the $g \to b\bar{b}$ signal process 150 000 events with gluon splitting to $b\bar{b}$ in the parton shower were generated with PYTHIA 6.130. This generator is used with a special option for gluon splitting to massive quarks, as explained in Sect. 4.1. All signal and background events were passed through a complete simulation of the OPAL detector [18].

The simulated events are weighted to correspond to the measured values of $c\bar{c}$ and $b\bar{b}$ production, $R_c = 0.1724$ and $R_b = 0.21664$, given in [19]. The rate of gluon splitting to $c\bar{c}$ pairs is set to $g_{c\bar{c}} = 3.20 \times 10^{-2}$ as measured by OPAL [20]. The ratio of the number of events with primary produced b quarks and $g \to c\bar{c}$ to the total number of events with $g \to c\bar{c}$ is fixed to the value predicted by JETSET 7.4.

In the following, simulated events with gluon splitting to $b\bar{b}$ signal are referred to as $g \to b\bar{b}$. They are further differentiated into events with a primary charm or light quark, referred to as $q\bar{q}b\bar{b}$ (q = udsc), and events with two $b\bar{b}$ quark pairs, referred to as $b\bar{b}b\bar{b}$.

Background to this analysis consists of various sources of four jet events. The dominant four-jet process is the production of two gluons in addition to the primary quarks, either from double Bremsstrahlung or from the triple gluon vertex. About 7% of the four-jet events are expected to be from gluon-splitting to a quark antiquark pair [21].

As this analysis is based on the identification of secondary decay vertices, there are two sources of background which have to be studied more carefully: events with gluon splitting to $c\bar{c}$ accompanied by any flavor of primary quark, and four-jet events with a primary $b\bar{b}$ quark pair but without gluon splitting to heavy quarks. They are referred to as $b\bar{b}xx$ (x = guds).

For comparisons to the data, the rate of gluon splitting to $b\bar{b}$ pairs is set to $g_{b\bar{b}} = 2.5 \times 10^{-3}$ and the rate of $b\bar{b}b\bar{b}$ events is set to $g_{4b} = 0.4 \times 10^{-3}$. Note that the rate $g_{b\bar{b}}$ includes $b\bar{b}b\bar{b}$ events. The fit procedure, described in Sect. 3.3, is completely independent of these two numbers.

2.4 The four-jet selection

The four-momenta of the selected tracks and clusters are combined to form four jets, using the $k_\perp$ (Durham) algorithm [22]. The value $y_{\rm cut}$ at which an event makes a transition between a three-jet and a four-jet assignment is denoted y_{34}. Figure 1 shows the normalized distribution of the quantity y_{34} for events that are selected as hadronic Z^0 decays, thereby comparing the data to the Monte Carlo prediction. In addition, the distribution predicted for $g \to b\bar{b}$ events is shown, scaled by a factor of 400. These events populate mainly the region of high y_{34}. A cut $y_{34} > 0.006$ is made to define the four-jet sample. This cut rejects nearly 90% of the background events, while retaining about 60% of the signal events. The estimated signal fraction assuming a signal rate $g_{b\bar{b}} = 2.5 \times 10^{-3}$ is 1.2%. In the data 443 334 events are selected, corresponding to 13.0% of all hadronic Z^0 decays. In the Monte Carlo simulation only 11.5% of the events are selected, because the prediction is slightly shifted to lower values of y_{34} with respect to the data. This corresponds to a deficit of $(11.7 \pm 0.2 \pm 0.8)$% four-jet events in the simulation compared to the data, where the first uncertainty is due to the finite number of events in the data and the simulation, the second is from the uncertainty in the rate of gluon splitting to $c\bar{c}$, $g_{c\bar{c}} = (3.20 \pm 0.43) \times 10^{-2}$ [20]. This deficit is attributed to missing higher orders in the parton shower simulation. To deal with this normalization problem, the number of simulated events is normalized to the number of four-jet events throughout this analysis, instead of normalizing to the number of hadronic Z^0 decays. The stability of this analysis with respect to variations of the cut in y_{34}, affecting this normalization, is discussed in Sect. 5.

2.5 Vertex reconstruction

A primary vertex is reconstructed for each event as described in [23]. Then for each jet a secondary vertex is reconstructed, using the full three-dimensional tracking information [24]. All tracks in the jet satisfying additional quality cuts on the momentum $p > 0.5\,\mathrm{GeV}/c$, the distance to the fitted primary vertex in the r/ϕ plane $d_0 < 0.3\,\mathrm{cm}$ and the uncertainty on d_0 of $\sigma_{d_0} < 0.1\,\mathrm{cm}$ are fitted to a common vertex. The relatively high momentum cut

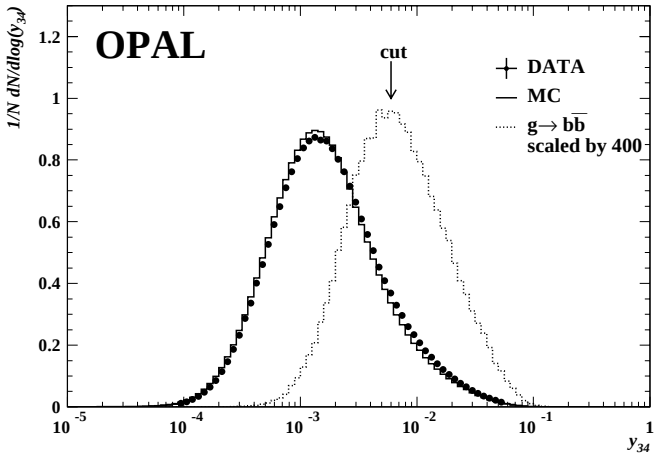

Fig. 1. Normalized distributions of the jet resolution parameter y_{34}. The data are shown with dots, the shape predicted from Monte Carlo simulations with a solid line and the shape predicted for the signal events as a dotted line

results in an increased contribution of tracks from the decay of b hadrons. Tracks with a large χ^2 contribution are removed from the vertex and the fit is repeated until the χ^2 contribution of each track is smaller than 4. If three or more tracks remain, the secondary vertex is accepted.

The decay length l and its error σ are calculated as the distance of the primary to the secondary vertex. The direction is constrained to be parallel to the jet axis. The decay length l is positive if the angle between the jet axis and the vector pointing from the primary to the secondary vertex is less than 90 degrees, negative otherwise. Vertices with $l > 0$ are used to identify b hadrons. In this analysis, the following variables are used to identify secondary vertices originating from the decay of b hadrons:

- The decay length significance l/σ, calculated from the decay length l and the experimental uncertainty σ on l. Secondary vertices significantly separated from the primary vertex are selected with a cut $l/\sigma > 3$.
- For the vertices surviving the $l/\sigma > 3$ cut the output *NN* of a neural network is calculated. This neural network has been trained to separate vertices originating from b hadron decays from those in charm or light quark events.

The neural network was developed for the OPAL $R_{\rm b}$ analysis [24]. It has five inputs: the decay length significance l/σ, the decay length l, the number of tracks in the secondary vertex n_s, the reduced decay length l_r/σ_r, where one well-defined track [24] has been removed from the vertex fit, and a variable x_D, sensitive to the invariant mass of the tracks in the jet that have a high probability of originating from a b hadron decay. The neural network output *NN* lies between zero and one. Values close to one indicate a high probability that the vertex is associated with a b hadron decay.

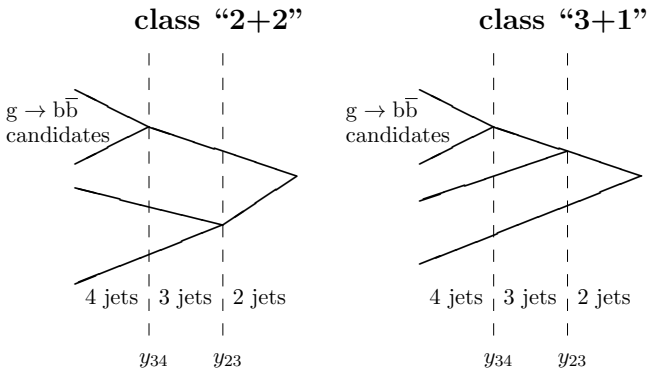

Fig. 2. Illustration of the definition of class "2+2" and class "3+1" and the $g \to b\bar{b}$ candidate jet selection

3 Analysis

In Sect. 3.1 the selection of candidate events for gluon splitting is described. By changing the y-cut and exploiting the transition from four to three jets, two jets are selected in each event as candidates to have originated from gluon splitting. The candidate jets are checked for secondary vertices and events with two significant secondary vertices are selected. The event sample is subdivided into two distinct classes, depending on the event topology. Optimized cuts on the neural network outputs are applied for each class, to define the candidate events. In Sect. 3.2 a dedicated selection of candidates for the process $Z^0 \to b\bar{b}b\bar{b}$ is discussed, where all four jets are checked for secondary vertices. Finally, in Sect. 3.3 the rate of gluon splitting to $b\bar{b}$ is calculated. For each of the selected event samples, angular distributions sensitive to four-quark final states are studied. The rates $g_{b\bar{b}}$ and g_{4b} are calculated using a binned maximum likelihood fit. The signal and background selection efficiencies and these angular distributions are used as input to the fit.

3.1 The $q\bar{q}b\bar{b}$ event selection

In each four-jet event the y-cut is increased, until the event changes to a three-jet event ($y_{\rm cut} > y_{34}$). The two jets that are combined in this step are considered as candidates for $g \to b\bar{b}$. The y-cut is then increased further, until the event changes to a two-jet event ($y_{\rm cut} > y_{23}$). There are two distinct possibilities for this, as shown in Fig. 2.

Class "2+2": Events belong to this class if none of the original four jets is identical to any of the two jets obtained after increasing the y-cut to force the event into a two-jet event.

Class "3+1": Events belong to this class if one of the original four jets is identical to one of the two jets obtained after increasing the y-cut to force the event into a two-jet event.

Monte Carlo studies show that events from the process $g \to b\bar{b}$ are preferentially selected in class "3+1". The corresponding selection efficiencies are given in Table 1. For a signal rate $g_{b\bar{b}} = 2.5 \times 10^{-3}$, in class "3+1" 1.47% of the events are from $g \to b\bar{b}$. In class "2+2" only 0.99% of the events are from $g \to b\bar{b}$. The event classification procedure selects 235 201 data events in class "2+2" and 208 133 in class "3+1". The Monte Carlo simulation predicts 240 774 and 202 560 events, respectively. Implications on the final result for $g_{b\bar{b}}$ and g_{4b} from this statistically significant difference in the number of observed to expected events in those two event classes are considered in the discussion of the experimental uncertainties.

The two $g \to b\bar{b}$ candidate jets selected in the first step are checked for secondary vertices. If both of these jets have a reconstructed secondary vertex with $l/\sigma > 3$, the event is selected. This cut is studied in Fig. 3a, where the decay length significance $(l/\sigma)_2$ of the second $g \to b\bar{b}$ candidate jet is shown. The two jets are ordered such that $(l/\sigma)_1 > (l/\sigma)_2$. If the variable $(l/\sigma)_2$ is larger than 3, the event is selected, otherwise it is rejected. Note that $(l/\sigma)_2 > 3$ implies $(l/\sigma)_1 > 3$. Because only the smaller decay length significance of the two vertices enters this distribution, there are many entries at negative $(l/\sigma)_2$ values. The cut $(l/\sigma)_2 > 3$ reduces the background from events with light flavors and it also reduces the fraction of events from the $g \to c\bar{c}$ process.

In the next step, the output of a neural network trained to recognize vertices from b hadron decays is calculated for the reconstructed vertices in the selected events. The two $g \to b\bar{b}$ candidates are ordered by their corresponding neural network output NN such that $NN_1 > NN_2$. The sum $NN_1 + NN_2$ shows good sensitivity to the signal process $g \to b\bar{b}$ for both event classes "2+2" and "3+1". It is depicted in Figs. 3b and 3c. To enrich the signal, cuts $NN_1 + NN_2 > 1.7$ in class "2+2" and $NN_1 + NN_2 > 1.1$ in class "3+1" are made. The cut values are chosen such as to obtain purities of about 40% for each class of events. Some discrepancies between data and the prediction are observed in Fig. 3 and in Table 1, mainly at low values of l/σ and low values of $NN_1 + NN_2$. These can be explained by uncertainties in the knowledge of the detector resolution, studied in Sect. 4.3.

Finally, the other two jets that were not considered to be gluon splitting candidates are checked for secondary vertices to gain some separation power for the $b\bar{b}b\bar{b}$ signal events. These jets are referred to as "primary quark jet candidates". If both of these jets have a vertex, only the jet with the larger decay length significance is considered. Figure 4 shows the distribution of the decay length significance of this reconstructed vertex, $(l/\sigma)_{\rm p}$, for the events selected from class "2+2" and "3+1". The variable $(l/\sigma)_{\rm p}$ shows some separation between the $b\bar{b}b\bar{b}$ events and the $q\bar{q}b\bar{b}$ (q = udsc) events. A cut at $(l/\sigma)_{\rm p} = 2$ is made to select event samples enriched or depleted with $b\bar{b}b\bar{b}$ events. The following four event samples are defined

Event sample A: Events from class "2+2" with $NN_1 + NN_2 > 1.7$ and $(l/\sigma)_{\rm p} > 2$, enriched in $b\bar{b}b\bar{b}$.

Event sample B: Events from class "2+2" with $NN_1 + NN_2 > 1.7$ not selected in sample A, depleted in $b\bar{b}b\bar{b}$.

Event sample C: Events from class "3+1" with $NN_1 + NN_2 > 0.7$ and $(l/\sigma)_{\rm p} > 2$, enriched in $b\bar{b}b\bar{b}$.

Table 1. Events selected at the different steps of the analysis (data), and the number of background (bgnd) and signal events expected from the simulation with $g_{b\bar{b}} = 2.5 \times 10^{-3}$ and $g_{4b} = 0.4 \times 10^{-3}$. Also shown are the efficiencies to select $q\bar{q}b\bar{b}$ (q = udsc) and $b\bar{b}b\bar{b}$ signal events, predicted from the Monte Carlo simulation

	Number of events				Selection efficiencies	
			signal			
	data	bgnd	$q\bar{q}b\bar{b}$	$b\bar{b}b\bar{b}$	$\epsilon_{q\bar{q}b\bar{b}}$	$\epsilon_{b\bar{b}b\bar{b}}$
The four-jet selection						
Total four-jet	443334	438191	4263	880	52.72%	56.95%
"2+2"	235201	238500	1901	373	23.51%	24.15%
"3+1"	208133	199691	2362	507	29.21%	32.80%
Event selection in Class "2+2"						
$(l/\sigma)_2 > 3$	613	596.2	51.2	17.8	0.63%	1.15%
$NN_1 + NN_2 > 1.7$	39	25.8	8.6	3.0	0.11%	0.20%
Sample A	14	6.3	1.2	2.2	0.02%	0.15%
Sample B	25	19.5	7.4	0.8	0.09%	0.05%
Event selection in Class "3+1"						
$(l/\sigma)_2 > 3$	359	310.6	71.4	22.3	0.88%	1.31%
$NN_1 + NN_2 > 1.1$	153	92.8	42.9	13.2	0.53%	0.85%
Sample C	44	40.1	6.7	9.6	0.08%	0.62%
Sample D	109	52.7	36.2	3.6	0.45%	0.23%
The dedicated $b\bar{b}b\bar{b}$ selection						
$(l/\sigma)_3 > 3$	628	642.8	18.0	55.8	0.22%	3.61%
remove overlap with A–D	589	604.6	14.0	46.0	0.17%	2.97%
Sample E	29	21.1	0.3	9.1	0.004%	0.59%
Selected (A–E)	221	139.7	51.8	25.3	0.64%	1.64%

Event sample D: Events from class "3+1" with $NN_1 + NN_2 > 0.7$ not selected in sample C, depleted in $b\bar{b}b\bar{b}$.

3.2 The dedicated $b\bar{b}b\bar{b}$ event selection

Starting again with the entire sample of four-jet events, selected with $y_{34} > 0.006$, a dedicated selection of $b\bar{b}b\bar{b}$ events is set up, independent of the cuts presented in the previous section. To find events with four b hadrons, events are selected where at least three decay vertices with a decay length significance $l/\sigma > 3$ are found. Figure 5a illustrates this selection of three significant vertices, showing the third largest decay length significance, denoted $(l/\sigma)_3$. The $b\bar{b}b\bar{b}$ signal is enhanced for large values of this variable. The cut $(l/\sigma)_3 > 3$ suppresses light flavors, most of the $g \to c\bar{c}$ events, and also the $q\bar{q}b\bar{b}$ (q = udsc) events. Figure 5b shows the third largest neural network output NN_3 for all selected vertices, where the events already selected in sample A–D are excluded to avoid double counting. The background dominates the region of low NN_3, while the $b\bar{b}b\bar{b}$ signal extends to high values of NN_3. A cut $NN_3 > 0.7$ is chosen to select the final $b\bar{b}b\bar{b}$ candidates from distribution, denoted as sample E.

3.3 Calculation of $g_{b\bar{b}}$ and g_{4b}

After applying all cuts, 221 events remain in the event samples A–E, where the simulation with $g_{b\bar{b}} = 2.5 \times 10^{-3}$ and $g_{4b} = 0.4 \times 10^{-3}$ predicts 217 ± 7 events. The efficiencies for selecting signal events, $q\bar{q}b\bar{b}$ (q = udsc) or $b\bar{b}b\bar{b}$ events, are denoted $\epsilon_{q\bar{q}b\bar{b}}$ and $\epsilon_{b\bar{b}b\bar{b}}$. The total efficiencies as obtained from the simulation are $\epsilon_{q\bar{q}b\bar{b}} = (0.64 \pm 0.02)\%$ and $\epsilon_{b\bar{b}b\bar{b}} = (1.64 \pm 0.07)\%$. The uncertainties quoted on the number of expected events and the selection efficiencies are due to the limited number of Monte Carlo events. Table 1 summarizes the number of selected events for the cuts applied, the number of signal and background events expected from the simulation, and the efficiencies to select signal or background reactions.

For the 221 signal events the angle α_{12-34} between two jet-jet planes is studied to distinguish signal events from the background, dominated by events with two quarks and two gluons. The first plane is spanned by the two jets that are joined into one jet by the jet-algorithm at the transition from four to three jets. The other plane is formed by the other two jets. The definition of this angle α_{12-34} is similar to the angular correlation proposed in [10] to measure the QCD color factors. In Fig. 6, the α_{12-34} dis-

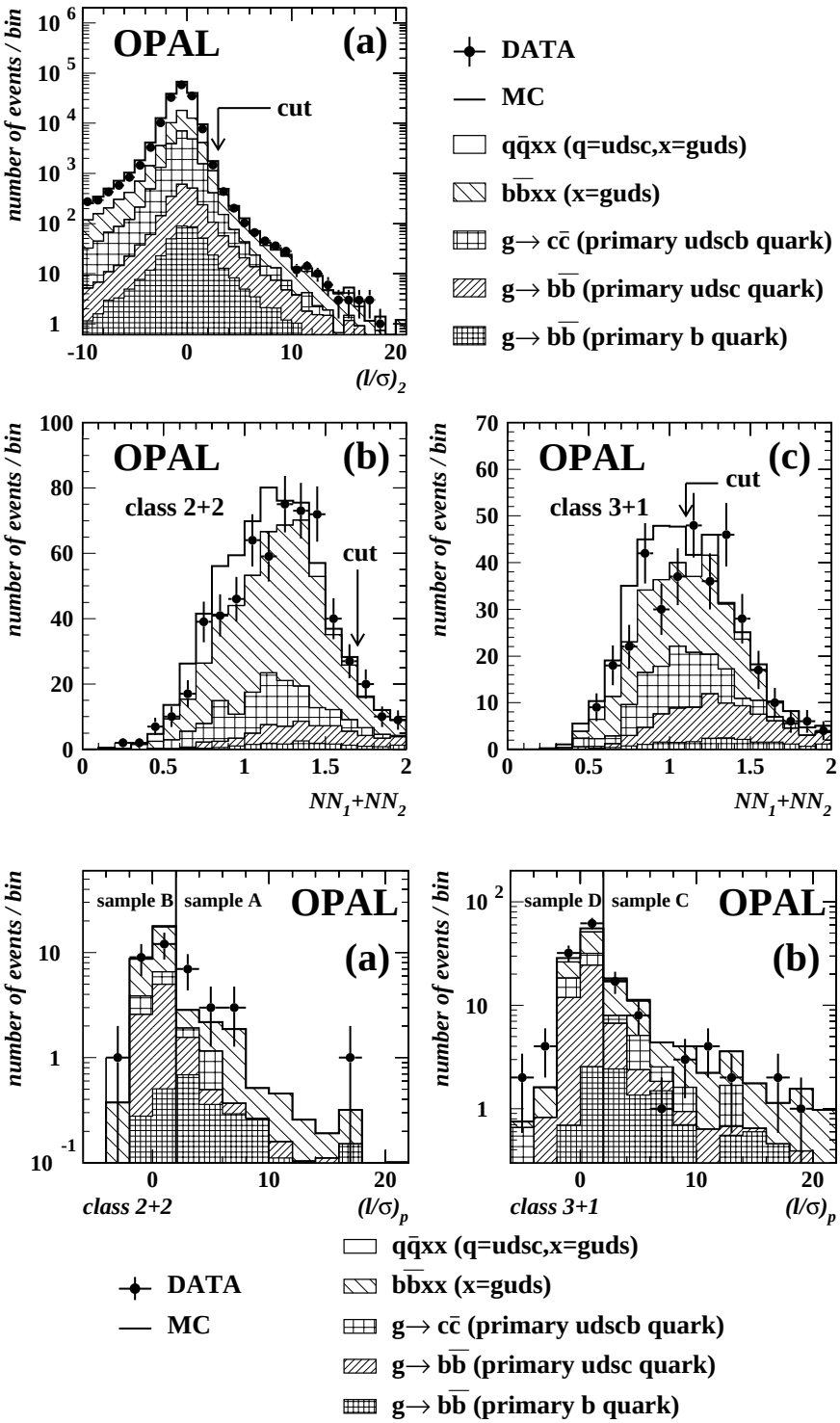

Fig. 3a–c. Variables used to select $g \to b\bar{b}$ candidate events. Plot **a** shows the decay length significance $(l/\sigma)_2$ of the $g \to b\bar{b}$ candidate jet with the smallest decay length significance. Plots **b** and **c** show the sum of the neural network outputs NN_1 and NN_2 for the events surviving the l/σ cut in class "2+2" and "3+1", respectively. The cut values are indicated by arrows. The points show data and the histogram shows the Monte Carlo simulation. The contributions from various four-jet processes are indicated

Fig. 4a,b. Largest decay length significance $(l/\sigma)_{\rm p}$ of the primary quark jet candidates, as defined in the text, after applying all selection cuts for the $q\bar{q}b\bar{b}$ selection. Events from class "2+2" appear in **a**, events from class "3+1" in **b**. The points show data and the histogram shows the Monte Carlo simulation. The contributions of various four-jet processes are indicated. The cut at $(l/\sigma)_{\rm p} = 2$ separating the event samples A from B and C from D is indicated

tribution is shown to be consistent with the theoretical prediction. The signal appears preferentially at high values of α_{12-34} while the background has a flatter distribution.

A maximum likelihood fit of the 26 bins in α_{12-34} shown in Fig. 6 is performed to extract $g_{\rm b\bar{b}}$ and $g_{\rm 4b}$, assuming Poisson distributions calculated from the signal and background efficiencies for each bin. The likelihood function is given by

$$-\ln\mathcal{L} = \sum_{i=1}^{26}(\mu_i - d_i \ln\mu_i) + \text{const},$$

where d_i is the number of observed events in bin i and μ_i is the corresponding number of predicted events (assumed to be the mean of the Poisson distributions). The latter is given by

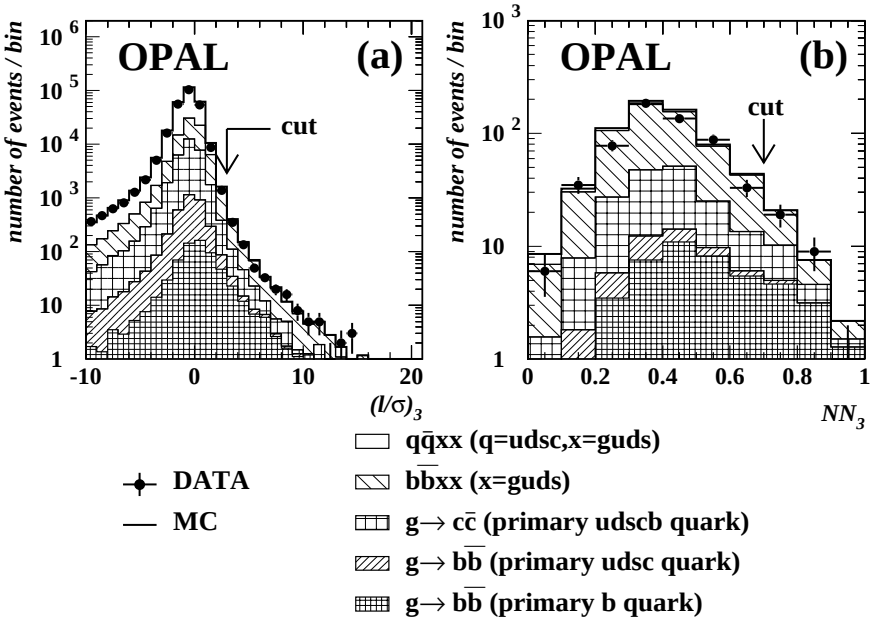

Fig. 5a,b. Variables used to select $b\bar{b}b\bar{b}$ events. Plot **a** shows the third largest decay length significance $(l/\sigma)_3$ of the four jets, plot **b** the third largest neural network output NN_3 with the cut $(l/\sigma)_3 > 3$ applied and the overlap with the event samples A-D removed. The points show data and the histogram shows the Monte Carlo simulation. The contributions from various four-jet processes are indicated. Arrows indicate the position of the cuts

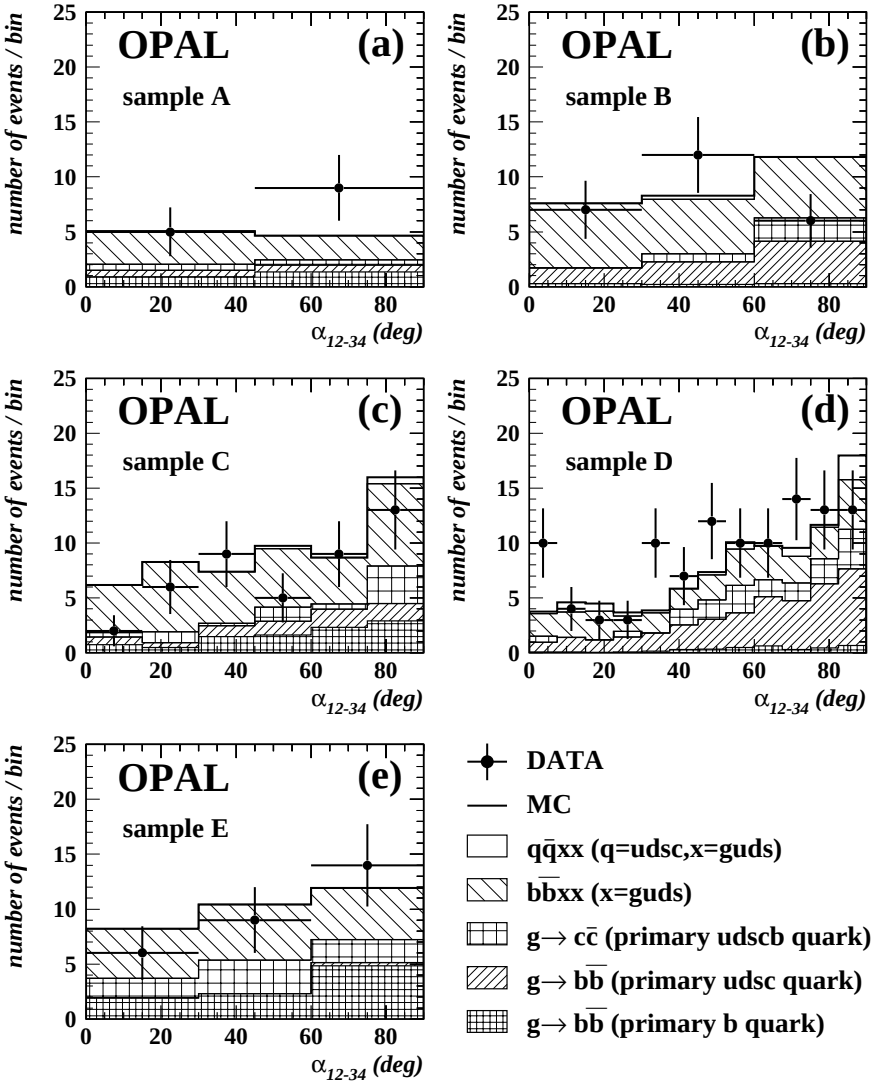

Fig. 6a–e. The angle α_{12-34} between the plane formed by the two $g \rightarrow b\bar{b}$ candidate jets and the plane formed by the other two jets for the $g \rightarrow b\bar{b}$ candidate events after applying all cuts. **a**–**e** correspond to the event samples A–E. The data are shown as full points with error bars, the Monte Carlo simulation as a solid line. The contributions from various four-jet processes are indicated

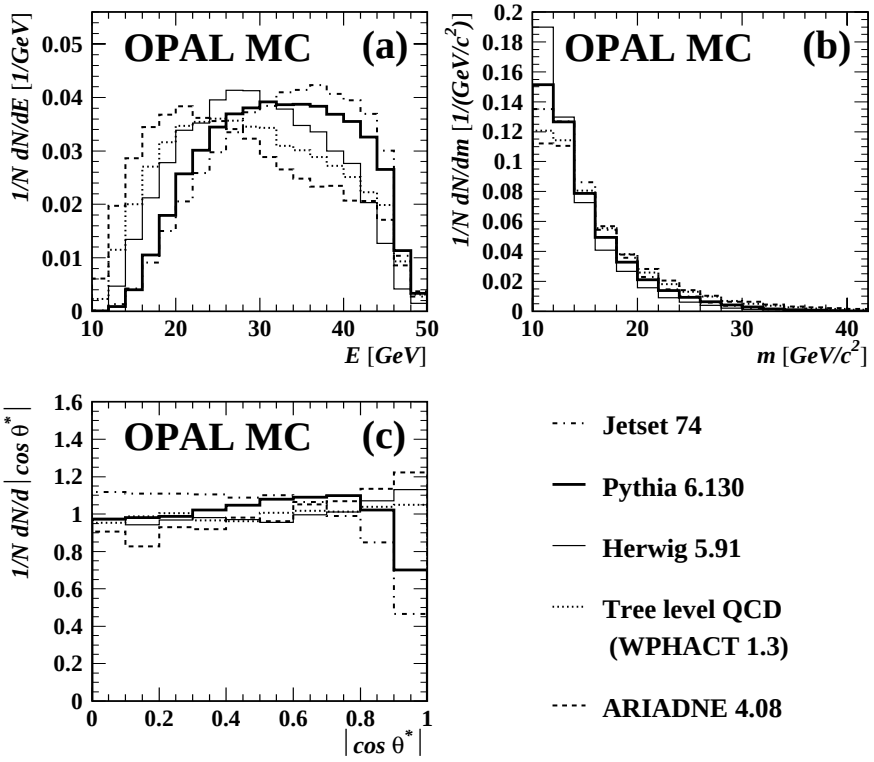

Fig. 7a–c. Normalized distributions of three kinematic variables of the gluon that splits to $b\bar{b}$ for different models and calculations, as described in the text: **a** the energy E, **b** the virtuality m, **c** the decay angle $|\cos\theta^\star|$ of the $b\bar{b}$ pair in the gluon rest frame

$$\begin{aligned}\mu_i = N_{4-\mathrm{jet}}\Big\{&(1-g_{c\bar{c}}-g_{b\bar{b}})\epsilon^i_{q\bar{q}}+g_{c\bar{c}}\epsilon^i_{q\bar{q}c\bar{c}}\\&+(g_{b\bar{b}}-g_{4b})\epsilon^i_{q\bar{q}b\bar{b}}+g_{4b}\epsilon^i_{b\bar{b}b\bar{b}}\Big\}\Big/\\&\Big\{(1-g_{c\bar{c}}-g_{b\bar{b}})\epsilon^{4-\mathrm{jet}}_{q\bar{q}}+g_{c\bar{c}}\epsilon^{4-\mathrm{jet}}_{q\bar{q}c\bar{c}}\\&+(g_{b\bar{b}}-g_{4b})\epsilon^{4-\mathrm{jet}}_{q\bar{q}b\bar{b}}+g_{4b}\epsilon^{4-\mathrm{jet}}_{b\bar{b}b\bar{b}}\Big\},\end{aligned}$$

where $N_{4-\mathrm{jet}}$ is the total number of selected four-jet events used for this analysis. The rate of gluon splitting to $c\bar{c}$ per hadronic Z^0 decay is denoted $g_{c\bar{c}}$. The two rates $g_{b\bar{b}}$ and g_{4b} are taken as the fit parameters. The probabilities to select the signal process for primary light quarks and the $b\bar{b}b\bar{b}$ events in bin i are denoted $\epsilon^i_{q\bar{q}b\bar{b}}$ and $\epsilon^i_{b\bar{b}b\bar{b}}$, while $\epsilon^i_{q\bar{q}c\bar{c}}$ and $\epsilon^i_{q\bar{q}}$ are the probabilities to select the $g \to c\bar{c}$ events or other background events in bin i. Finally $\epsilon^{4-\mathrm{jet}}_{q\bar{q}b\bar{b}}$, $\epsilon^{4-\mathrm{jet}}_{b\bar{b}b\bar{b}}$, $\epsilon^{4-\mathrm{jet}}_{q\bar{q}c\bar{c}}$, $\epsilon^{4-\mathrm{jet}}_{q\bar{q}}$ are the efficiencies for events in the signal and the background channels to pass the four-jet selection. The likelihood analysis leads to the result

$$\begin{aligned}g_{b\bar{b}} &= (3.07 \pm 0.53)\times 10^{-3},\\ g_{4b} &= (0.36 \pm 0.17)\times 10^{-3},\end{aligned}$$

with a correlation coefficient between $g_{b\bar{b}}$ and g_{4b} of $+0.007$. The errors are statistical only.

4 Evaluation of systematic uncertainties

Various sources of systematic uncertainties are considered, as summarized in Table 2 and discussed in the following. Additional cross-checks are presented in Sect. 5.

4.1 Model dependence

Though the parton shower approach as implemented in JETSET 7.4 is expected to describe the gluon splitting process quite well [1], it is desirable to look at various alternative models and at exact calculations. In PYTHIA 6.130 [17], using the option `MSTJ(42)=3`, the calculation of the opening angle in the gluon splitting process has been modified to take mass effects into account, as compared to JETSET 7.4. The PYTHIA 6.130 prediction for the $g \to b\bar{b}$ process is used to evaluate the main results of this analysis. The HERWIG 5.91 [25] Monte Carlo generator[2] provides an alternative model for the parton shower. Another approach is given by the Color Dipole Model, using the event generator ARIADNE 4.08 [26].

The program WPHACT [9] implements e^+e^- annihilation to four fermions, where the masses of b quarks are taken into account for the calculation of the matrix elements. It can be used to study $b\bar{b}b\bar{b}$ and $b\bar{b}q\bar{q}$ final states. Version 1.3 of WPHACT[3] [27] allows for the possibility to switch off Feynman graphs where the b quarks couple to the Z^0 or γ, enabling studies of the gluon splitting process at tree level. For the case of primary light quarks, calculations are available including next-to-leading order logarithmic terms [1,2]. The shapes of the WPHACT 1.3 predictions are in agreement with these calculations in the regions where such a comparison is possible.

Figure 7 shows differential distributions of kinematic variables of the gluon that splits to $b\bar{b}$, calculated with PYTHIA 6.130,JETSET 7.4, HERWIG 5.91, ARIADNE 4.08

[2] This version was already used in [7]

[3] Provided to us by courtesy of the author

Table 2. Summary of the systematic uncertainties on the rates $g_{b\bar{b}}$ and g_{4b} and the corresponding correlations

Source of systematic error	$\Delta g_{b\bar{b}} \times 10^3$	$\Delta g_{4b} \times 10^3$	Correlation
Model dependence	0.72	0.17	+1
b quark mass	0.23	0.03	+1
Monte Carlo statistics	0.28	0.09	−0.07
Detector simulation	0.23	0.15	+1
Event classification	0.18	0.03	+1
Flavor composition R_b^{4-jet}	0.07	0.02	+1
Gluon splitting to charm $g_{c\bar{c}}$	0.05	0.01	+1
Bottom fragmentation	0.39	0.10	+0.86
Bottom decay multiplicities	0.11	0.03	+1
Bottom production rates	0.11	0.01	+0.70
Bottom hadron lifetimes	0.11	0.05	+0.09
Charm fragmentation	0.07	0.03	−0.52
Charm decay multiplicities	0.03	0.01	+0.96
Charm production rates	0.02	0.01	−0.97
Charm hadron lifetimes	0.05	0.01	+0.80
Total systematic error	**0.97**	**0.27**	**+0.78**

Table 3. Results obtained for various Monte Carlo models

Model	Implementation	$g_{b\bar{b}} \times 10^3$	$g_{4b} \times 10^3$
Jetset 7.4	Full detector simulation	2.35 ± 0.41	0.34 ± 0.17
Pythia 6.130 (default)	Full detector simulation	3.07 ± 0.53	0.36 ± 0.17
Wphact 1.3	Event reweighting	3.22 ± 0.58	0.31 ± 0.15
Herwig 5.91	Event reweighting	3.38 ± 0.59	0.40 ± 0.19
Ariadne 4.08	Event reweighting	3.62 ± 0.64	0.36 ± 0.19

and Wphact 1.3. The "gluon" variables have been calculated from the $b\bar{b}$ quark pair at the end of the shower. For the case of $b\bar{b}b\bar{b}$ events the $b\bar{b}$ quark pair with the lowest invariant mass is chosen. The hardest energy spectrum is predicted by Jetset 7.4, while Ariadne 4.08 leads to the softest energy spectrum, when comparing the five models. For the gluon virtuality the Ariadne 4.08 prediction leads to the hardest distribution, while Herwig 5.91 predicts the softest spectrum. For the decay angle in the gluon rest frame the models differ most significantly at high $|\cos\theta^\star|$. The extreme cases are covered by Jetset 7.4 with a low number of events in this region and by Ariadne 4.08 showing an enhancement of events with increasing $|\cos\theta^\star|$. Note that the Pythia 6.130 prediction is always well between those extreme cases, this is why we decided to use it for the main analysis results.

To study hadronisation and detector effects, we use two sets of events generated either with Jetset 7.4 or with Pythia 6.130, and having a detailed hadronisation and detector simulation. The Jetset 7.4 sample is only used for systematic checks.

The differential efficiencies to select the signal events, $q\bar{q}b\bar{b}$ ($q = udsc$) and $b\bar{b}b\bar{b}$ in this analysis, are shown in Fig. 8. They are evaluated with the Pythia 6.130 event sample. The efficiencies are low for small gluon energies E and gluon virtualities m, as it is difficult to detect the two b hadrons in two separate jets in this region. The same is true for decay angles $|\cos\theta^\star|$ close to one, because in this case the two b hadrons have a small transverse momentum relative to the gluon flight direction.

To evaluate model-dependent effects, the complete analysis chain is performed using either the Pythia 6.130 or the Jetset 7.4 event sets. In addition, the Pythia 6.130 events are weighted such as to reproduce the gluon distributions from Fig. 7 predicted by Herwig 5.91, Ariadne 4.08 and Wphact 1.3, and the analysis is repeated. Table 3 summarizes the individual results of these studies. To study possible deficiencies in the reweighting procedure, it is repeated based on the Jetset 7.4 event sample rather than on the Pythia 6.130 event sample. This results in slightly lower values of $g_{b\bar{b}}$ and larger values of g_{4b}, as compared to the Herwig 5.91, Ariadne 4.08 and Wphact 1.3 values shown in Table 3. The most significant differences to the standard reweighting procedure are observed for Herwig 5.91, namely $g_{b\bar{b}} = 2.88 \times 10^{-3}$ and $g_{4b} = 0.53 \times 10^{-3}$.

Finally, the largest differences on $g_{b\bar{b}}$ and g_{4b} to the central value are taken as systematic uncertainty due to

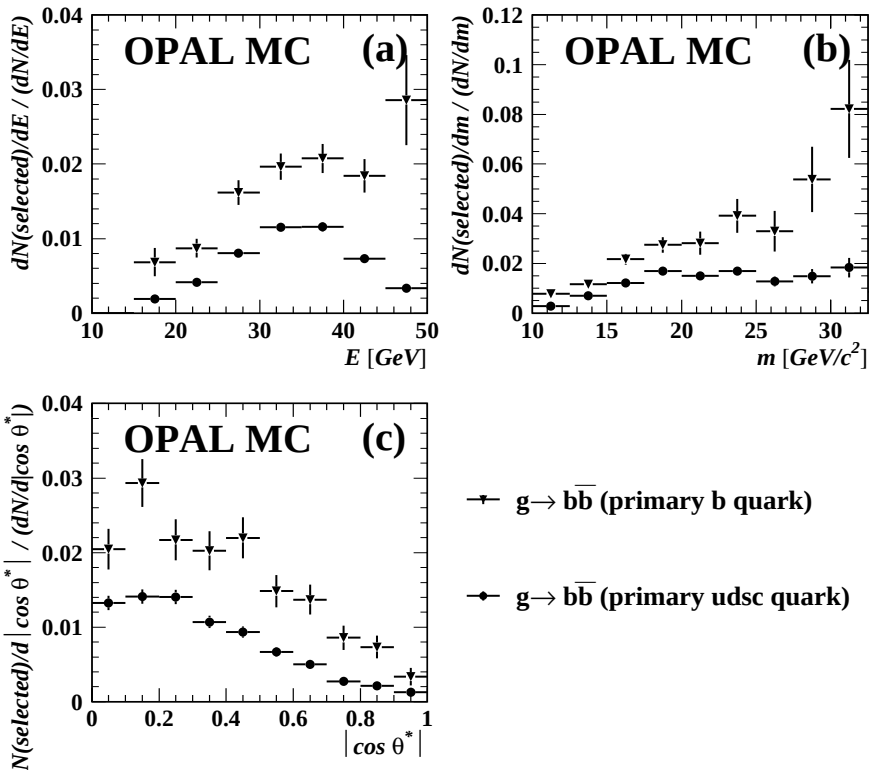

Fig. 8a–c. Selection efficiencies as a function of kinematic variables of the gluon that splits to $b\bar{b}$: **a** the energy E, **b** the virtuality m, **c** the decay angle $|\cos\theta^\star|$ of the $b\bar{b}$ pair in the gluon rest-frame. The efficiencies to select $q\bar{q}b\bar{b}$ (q = udsc) and $b\bar{b}b\bar{b}$ events are indicated

limited knowledge of the gluon splitting mechanism. For $g_{b\bar{b}}$ this is the PYTHIA 6.130–JETSET 7.4 difference, while for g_{4b} this is the PYTHIA 6.130–HERWIG 5.91 difference, where the HERWIG 5.91 result is calculated with the help of reweighted JETSET 7.4 events.

4.2 Dependence on the b quark mass

The influence of the b quark mass assumed for the Monte Carlo simulation has been studied by changing the b quark mass in the PYTHIA 6.130 program[4] and investigating the properties of the b hadrons produced in the fragmentation process. The central value for the b quark mass in PYTHIA 6.130 used throughout this analysis is $5\,\mathrm{GeV}/c^2$. The shapes of the distributions of various kinematic variables are used to reweight the $g \to b\bar{b}$ Monte Carlo events corresponding to a b quark mass of $4.5\,\mathrm{GeV}/c^2$ and $5.25\,\mathrm{GeV}/c^2$. This variation covers the uncertainty of the b quark pole mass [28] up to the B meson mass. Note that the way the quark mass parameter is used in PYTHIA 6.130 corresponds rather to a constituent quark mass than to a pole mass definition of the quark mass [29], which justifies the choice of $5\,\mathrm{GeV}/c^2$ for the central value.

The quantities used for the reweighting process are the momenta of the two b hadrons produced in the fragmentation process and their invariant mass. These variables are chosen because the efficiency to identify b hadrons strongly depends on their momentum. The efficiency to resolve the two b hadrons in different jets depends on their invariant mass. The larger deviations from the standard results are found for a b quark mass of $4.5\,\mathrm{GeV}/c^2$. They are taken into account as systematic uncertainties.

4.3 Experimental sources of systematic uncertainties

The modeling of the OPAL detector is important because the analysis depends on an accurate understanding of the decay vertex reconstruction. The b tagging efficiencies are mainly sensitive to the parameters modeling the production and decay of b hadrons. This will be discussed in Sect. 4.4. The light quark tagging efficiencies in the Monte Carlo simulation are mainly sensitive to details in the modeling of the tracking system. Studies are done by increasing the difference of the reconstructed track parameters with respect to the true track parameters in the Monte Carlo simulation by 10% to cover uncertainties in the knowledge of the flavor tagging variables [24]. This smearing is applied separately for parameters defined in the (r,ϕ) and the (r,z) plane. In (r,ϕ) a simultaneous smearing of the distance of closest approach, d_0, and the azimuthal angle ϕ_0 is performed. In (r,z) smearing is done simultaneously for the z coordinate of the point of closest approach in (r,ϕ) and the polar angle θ. Finally the gluon splitting analysis is repeated using the modified Monte Carlo sets. The uncertainties from the smearing in (r,ϕ) and (r,z) are added quadratically.

The normalization to the number of four-jet events revealed differences in the population of the event classes "2+2" and "3+1"when comparing the data with the Monte Carlo prediction, as discussed in Sect. 3.1. This is

[4] The relevant parameter in the PYTHIA 6.130 program is `PMAS(5,1)`

addressed by repeating the likelihood fit, using the numbers of events and selection efficiencies of the "2+2" and "3+1" classes, rather than the number of four-jet events with their corresponding selection efficiencies. The variation found is assigned as systematic uncertainty due to the event classification.

4.4 Uncertainties from heavy flavor physics

The rate of primary $b\bar{b}$ production in the four-jet sample $R_b^{4-\mathrm{jet}}$ can be measured using a double-tag technique. Agreement with the Monte Carlo simulation within 2.4% is found, where the statistical uncertainties are in the order of 1.5%. The rate $R_b^{4-\mathrm{jet}}$ in the Monte Carlo sample has been changed by 2.4% and the differences in $g_{b\bar{b}}$ and g_{4b} to our standard results are taken as systematic uncertainties. Varying the rate of primary $c\bar{c}$ production R_c within its uncertainties only has a negligible effect on the results.

The rate of secondary $c\bar{c}$ quark pairs from gluons, $g_{c\bar{c}}$, has been measured by OPAL to be $g_{c\bar{c}} = (3.20 \pm 0.43) \times 10^{-2}$ [20]. This measurement is based on lepton identification and the reconstruction of $D^\star$ mesons in three-jet events. It can be considered as statistically independent of the $g_{b\bar{b}}$ measurement presented here, which is based on lifetime-tags in four-jet events. The rate $g_{c\bar{c}}$ thus is varied within its uncertainty to obtain systematic uncertainties on $g_{b\bar{b}}$ and g_{4b}. The explicit dependence of the results of this analysis on $g_{c\bar{c}}$ is given by

$$\frac{\Delta g_{b\bar{b}}}{g_{b\bar{b}}} = -0.125 \times \frac{\Delta g_{c\bar{c}}}{g_{c\bar{c}}}, \quad \frac{\Delta g_{4b}}{g_{4b}} = -0.259 \times \frac{\Delta g_{c\bar{c}}}{g_{c\bar{c}}}.$$

The fragmentation functions for charm and bottom quarks are varied to reflect the uncertainties in the knowledge of the average scaled energies for D and B mesons, $\langle x_E \rangle_c = 0.484 \pm 0.008$ and $\langle x_E \rangle_b = 0.702 \pm 0.008$ [31]. This is done by varying the parameter ϵ in the parameterization of the fragmentation function suggested by Peterson et. al. [32]. In addition the sensitivity to the shape of the fragmentation function is checked, using the models suggested by Collins and Spiller [33] and Kartvelishvili [34]. The parameters of these models are chosen to reproduce the measured values of the mean scaled energies of the D and B mesons in the Monte Carlo simulation, and the larger deviations in $g_{b\bar{b}}$ and g_{4b} are used as systematic uncertainties from this source. The uncertainties from the knowledge of the mean scaled energies and the shape of the distributions are added in quadrature.

The charged decay multiplicities of the D mesons are varied within the errors given in [35] around the JETSET 7.4 prediction. Particles from decay-chains of b hadrons are excluded from this variation. The mean charged decay multiplicity of weakly decaying b hadrons is varied within $n_B = 4.995 \pm 0.062$ [31]. This multiplicity includes secondary decays of charm hadrons produced in the decay chains. Variations of the neutral decay multiplicities have not been studied, but are expected to be small.

The production rates of charm and bottom hadrons in the Monte Carlo simulation are varied within the ranges given by the LEP Electroweak Working group [31] and the Particle Data Group [28], respectively. This variation includes particles from primary $b\bar{b}$ and $c\bar{c}$ production as well as those from gluon splitting to heavy quarks.

The lifetimes of charm and bottom hadrons are varied around their central value according to the numbers given by the Particle Data Group [28].

4.5 Results

All contributions to the systematic uncertainties are added in quadrature, leading to the results

$$g_{b\bar{b}} = (3.07 \pm 0.53(\mathrm{stat.}) \pm 0.97(\mathrm{syst})) \times 10^{-3},$$
$$g_{4b} = (0.36 \pm 0.17(\mathrm{stat.}) \pm 0.27(\mathrm{syst})) \times 10^{-3}.$$

The systematic errors on $g_{b\bar{b}}$ and g_{4b} have a correlation +0.78. This large positive correlation can be understood from the fact that most of the systematic variations influence the selection efficiencies for both the $g \to b\bar{b}$ and the $b\bar{b}b\bar{b}$ signal in the same direction.

5 Additional cross-checks

The four-jet selection is defined using a cut $y_{34} > y_{34}^{\min}$. Figure 9a shows the number of events in the data divided by the predicted number of events as a function of this cut. The disagreement in the rate of four-jet events, as discussed in Sect. 2.4, is clearly visible. The fit results for $g_{b\bar{b}}$ and g_{4b} as a function of this cut are studied in Fig. 9b and 9c. The fit results are stable under the variation of $y_{34}^{\min}$ within the independent statistical error. Note that the variation of $y_{34}^{\min}$ from 0 to 0.014 corresponds to a variation in the number of candidate events from 1003 to 93 and a variation of the estimated $g \to b\bar{b}$ signal purity from 10% to 50%. These checks show that the treatment of the normalization to the four-jet rate in the likelihood fit is correct.

To check the fitting procedure a likelihood fit is applied to the normalized signal and background shapes in α_{12-34}, calculating directly the fractions of $q\bar{q}b\bar{b}$ (q = udsc) and $b\bar{b}b\bar{b}$ events in the final event selection from these shapes. Using the number of selected events, the total number of hadronic Z^0 decays and the signal efficiencies, $g_{b\bar{b}}$ and g_{4b} can be calculated from these event fractions. This procedure avoids the need to know the absolute selection efficiency for the background. Alternatively, the likelihood fit is repeated using only the individual signal and background selection efficiencies of the event samples A–E. This analysis is thus independent of the variable α_{12-34}. Both results are compatible with the default method.

The $k_\perp$ algorithm is used in this analysis not only to define the jets, but also to define the event topology. Therefore it is important to test the analysis, using a different algorithm. The JADE E0 [30] jet clustering scheme is used as an alternative method. Four-jet events are selected with a cut $y_{34}^{JADE} > 0.015$, resulting in a similar number of four-jet events as compared to the default analysis which is based on the $k_\perp$ algorithm. To

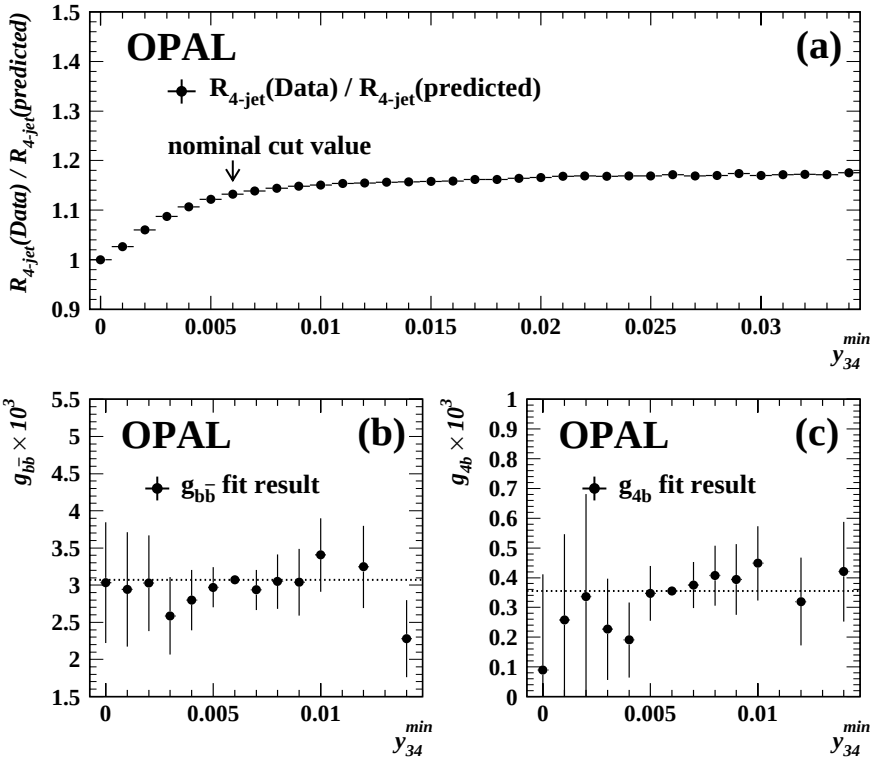

Fig. 9a–c. Dependence of the four-jet rate $R_{4-\mathrm{jet}}$ and the fit results on $y_{34}^{\min}$, the lower cut in the jet resolution parameter y_{34}. **a** shows the ratio of the number of events in the data by the number of events predicted from the Monte Carlo simulation, **b** and **c** show the fit result for $g_{\mathrm{b\bar{b}}}$ and $g_{4\mathrm{b}}$. The error bars in **b** and **c** correspond to the statistical errors independent of the central value $y_{34}^{\min} = 0.006$

classify the events and define the gluon splitting candidates, as described in Sect. 3.1, and to define the angle α_{12-34}, as described in Sect. 3.3, the new definition of the jet resolution parameter in the JADE E0 scheme is used. All other analysis cuts are unchanged with respect to the standard analysis. This results in 207 selected events. The result of the likelihood fit using the JADE E0 algorithm is $g_{\mathrm{b\bar{b}}}^{\mathrm{JADE}} = (3.11 \pm 0.59) \times 10^{-3}$ and $g_{4\mathrm{b}}^{\mathrm{JADE}} = (0.45 \pm 0.17) \times 10^{-3}$ (statistical uncertainties only). These results are compatible with the results obtained with the $k_\perp$ algorithm within the statistical errors, considering the small fraction of events common to both selections.

6 Summary

A measurement of the inclusive rate of gluon splitting to $b\bar{b}$ per hadronic Z^0 decay has been performed using data taken by OPAL. The result is

$$g_{\mathrm{b\bar{b}}} = (3.07 \pm 0.53 \pm 0.97) \times 10^{-3}.$$

The rate of events with four bottom quarks is measured simultaneously, with the result

$$g_{4\mathrm{b}} = (0.36 \pm 0.17 \pm 0.27) \times 10^{-3}.$$

The correlation of $g_{\mathrm{b\bar{b}}}$ and $g_{4\mathrm{b}}$ is $+0.007$ from statistical uncertainties and $+0.78$ from systematic uncertainties. The ratio $g_{4\mathrm{b}}/g_{\mathrm{b\bar{b}}}$ is thus measured to be

$$\frac{g_{4\mathrm{b}}}{g_{\mathrm{b\bar{b}}}} = 0.116 \pm 0.060 \pm 0.065.$$

This is in agreement with the simplified expectation $g_{4\mathrm{b}}/g_{\mathrm{b\bar{b}}} \approx R_{\mathrm{b}}$ and with a more detailed calculation performed by DELPHI [8], predicting $g_{4\mathrm{b}}/g_{\mathrm{b\bar{b}}} = 0.1833 \pm 0.0003$. The results for $g_{\mathrm{b\bar{b}}}$ and $g_{4\mathrm{b}}$ are compatible with previous measurements [6–8] as well as theoretical predictions [1, 4].

Acknowledgements. We particularly wish to thank the SL Division for the efficient operation of the LEP accelerator at all energies and for their continuing close cooperation with our experimental group. We thank our colleagues from CEA, DAPNIA/SPP, CE-Saclay for their efforts over the years on the time-of-flight and trigger systems which we continue to use. In addition to the support staff at our own institutions we are pleased to acknowledge the Department of Energy, USA, National Science Foundation, USA, Particle Physics and Astronomy Research Council, UK, Natural Sciences and Engineering Research Council, Canada, Israel Science Foundation, administered by the Israel Academy of Science and Humanities, Minerva Gesellschaft, Benoziyo Center for High Energy Physics, Japanese Ministry of Education, Science and Culture (the Monbusho) and a grant under the Monbusho International Science Research Program, Japanese Society for the Promotion of Science (JSPS), German Israeli Bi-national Science Foundation (Fig), Bundesministerium für Bildung und Forschung, Germany, National Research Council of Canada, Research Corporation, USA, Hungarian Foundation for Scientific Research, OTKA T-029328, T023793 and OTKA F-023259.

References

1. M. H. Seymour, Nucl. Phys. **B436** (1995) 163–183
2. D. J. Miller, M. H. Seymour, Phys. Lett. **B435** (1998) 213
3. T. Sjöstrand, Comp. Phys. Comm. **39** (1986) 347; T. Sjöstrand, Comp. Phys. Comm. **82** (1994) 74
4. S. Frixione et al., CERN-TH-97-16, publ. in: Heavy Flavours 2, A. J. Buras (ed.) and M. Lindner (ed.), Singapore World Sci. (1998)
5. B. A. Kniehl, J. H. Kühn, Nucl. Phys. **B329** (1990) 547–573
6. DELPHI Collaboration, P. Abreu et al., Phys. Lett. **B405** (1997) 202
7. ALEPH Collaboration, R. Barate et al., Phys. Lett. **B434** (1998) 437
8. DELPHI Collaboration, P. Abreu et al., Phys. Lett. **B462** (1999) 425
9. E. Accomando, A. Ballestrero, Comp. Phys. Comm. **99** (1997) 270
10. M. Bengtsson, P. Zerwas, Phys. Lett. **B208** (1988) 306
11. OPAL Collaboration, K. Ahmet et al., Nucl. Instr. Meth. **A305** (1991) 275
12. P. P. Allport et al., Nucl. Instr. and Meth. **A324** (1993) 34
13. P. P. Allport et al., Nucl. Instr. and Meth. **A346** (1994) 476
14. S. Anderson et al., Nucl. Instr. and Meth. **A403** (1998) 326
15. OPAL Collaboration, G. Alexander et al., Z. Phys. **C52** (1991) 175
16. OPAL Collaboration, K. Ackerstaff et al., Eur. Phys. J. **C2** (1998) 213
17. T. Sjöstrand, update release notes (Internet communication of May 22, 2000: `http://www.thep.lu.se/torbjorn/Pythia.html`)
18. J. Allison et al., Nucl. Instr. and Meth. **A317** (1992) 47
19. The LEP Electroweak Working group, CERN-EP/99-015
20. OPAL Collaboration, G. Abbiendi et al., Eur. Phys. J. **C13** (2000) 1
21. DELPHI Collaboration, P. Abreu et al., Z. Phys. **C59** (1993) 357
22. S. Catani et al., Phys. Lett. **B269** (1991) 432; N. Brown and W. J. Stirling, Z. Phys. **C53** (1992) 629
23. OPAL Collaboration, K. Ackerstaff et al., Z.Phys. **C74** (1997) 1
24. OPAL Collaboration, G. Abbiendi et al., Eur. Phys. J. **C8** (1999) 217
25. G. Marchesini, B. R. Webber, G. Abbiendi, I. G. Knowles, M. H. Seymour, L. Stanco, Comp. Phys. Comm. **67** (1992) 465; M. H. Seymour, private communication
26. L. Lönnblad, Comp. Phys. Comm. **71** (1992) 15
27. A. Ballestrero, private communication
28. Particle Data Group, C. Caso et al., Eur. Phys. J. **C3** (1998) 1
29. T. Sjöstrand, private communication
30. JADE collaboration, W. Bartel et al., Z. Phys. **C33** (1986) 23; JADE collaboration, S. Bethke et al., Phys. Lett. **B213** (1988) 235
31. The LEP collaborations, ALEPH, DELPHI, L3 and OPAL, Nucl. Instr. Meth. **A378** (1996) 101; Updated averages as described in 'Presentation of LEP Electroweak Heavy Flavour Results for Summer 1998 Conferences', LEPHF 98-01 (Internet communication of May 22, 2000: `http://www.cern.ch/LEPEWWG/heavy/`)
32. C. Peterson, D. Schlatter, I. Schmitt, P. Zerwas, Phys. Rev. **D27** (1983) 105
33. P. Collins, T. Spiller, J. Phys. **G11** (1985) 1289
34. V. G. Kartvelishvili, A. K. Likhoded, V. A. Petrov, Phys. Lett. **B78** (1978) 615
35. MARK III collaboration, D. Coffman et al., Phys. Lett. **B263** (1991) 135